WATER RESOURCES RESEARCH, VOL. 31, NO. 7, PAGES 1637–1646, JULY 1995

Effect of solute size on transport in structured porous media

Qinhong Hu and Mark L. Brusseau

Department of Soil and Water Science, University of Arizona, Tucson

Abstract. The purpose of this work was to investigate the effect of solute size on transport in structured porous media. Miscible displacement experiments were performed with tracers of different sizes (i.e., tritiated water (^3H_2O), pentafluorobenzoate (PFBA), 2,4-dichlorophenoxyacetic acid (2,4-D), and hydroxypropyl-β-cyclodextrin (HPCD)) in aggregated, stratified, and macroporous media. The breakthrough curves exhibited both early breakthrough and tailing, indicative of nonideal transport in these structured media. Comparison of breakthrough curves revealed that the extent of nonideality (e.g., tailing) was HPCD > PFBA, 2,4-D > ^3H_2O. This behavior is consistent with the impact of solute size on the relative degree of "nonequilibrium" experienced by solutes whose transport is constrained by diffusive mass transfer. The capability of the first-order, dual-porosity mobile-immobile model to represent solute transport in these structured systems was evaluated by comparing independently determined values of the input parameters to values obtained by curve fitting of the experimental measurements. The calculated and optimized values compared quite well for the aggregated and stratified media, but not for the macroporous media. Experiments performed with tracers of different size are useful for characterizing the nature of the porous medium through which transport is occurring.

Introduction

The transport of solute in structured and heterogeneous porous media is a problem that has great import for issues such as the probability of groundwater's becoming contaminated and remediation of contaminated sites. The impact of structured media on the transport of dissolved chemicals has been studied by many researchers [see *Biggar and Nielsen*, 1962; *Passioura*, 1971; *van Genuchten and Wierenga*, 1977; *Rao et al.*, 1980b; *Nkedi-Kizza et al.*, 1983; *Sudicky et al.*, 1985; *Southworth et al.*, 1987; *Herr et al.*, 1989; *Brusseau and Rao*, 1990; *Singh and Kanwar*, 1991; *Czapar et al.*, 1992; *Koch and Flühler*, 1993; *Brusseau*, 1993; *Brusseau et al.*, 1994]. These investigations have shown that the presence of macroscopic-scale low-permeability domains (e.g., aggregates, stratified layers, and the matrix of macroporous structured soil) can cause nonideal transport of solutes, as exemplified by asymmetrical breakthrough curves and "preferential" transport.

A major characteristic of many structured media is the existence of preferential flow paths wherein advection dominates transport. Rapid transport in the "advective" domains is accompanied by diffusive mass transfer of solutes between domains that are advection dominated and those that are not. The "nonadvective" domains, therefore, behave as sink/source components. Hence, in these systems access to portions of the porous medium is constrained by diffusive mass transfer. In such systems, differences in transport should be observed for solutes with different sizes, given the relationship between size (e.g., molecular weight) and diffusivity. This aspect of solute transport has received little attention to date.

The purpose of this research is to investigate the transport of nonreactive solutes with different sizes in saturated, constructed structured media (aggregated, stratified, and macroporous media). Data obtained from miscible displacement experiments will be used to examine the effect of solute size on nonideal transport. The dual-porosity mobile-immobile model will be used to attempt to quantify the solute size effect.

Paper number 95WR01138.
0043-1397/95/95WR-01138$05.00

Materials and Methods

Materials

Analytical grade pentafluorobenzoate (PFBA) and 2,4-dichlorophenoxyacetic acid (2,4-D) (>99% purity) were purchased from Aldrich Chemical Company. The modified cyclodextrin, hydroxypropyl-β-cyclodextrin (HPCD), with a hydrophilic shell and a relatively apolar cavity (structure reported by *Wang and Brusseau* [1993]), was selected for its larger molecular weight and relatively large solubility. It was also purchased from Aldrich, with no purity reported. Tritiated water was purchased from New England Nuclear. The pertinent properties of solutes are listed in Table 1.

Experimental Procedures

Aggregated system. The synthetic aggregated porous media used in this study consisted of porous spheres with radii of 0.55 cm. Details of the technique employed to prepare the water-stable spheres from kaolinite clay suspension were described by *Rao et al.* [1980a]. The average porosity of these spheres is about 0.365 cm^3/cm^3. Analysis by scanning electron microscopy (SEM) showed that the spheres (both at the surface and down to the center) are composed of pores that are about 1 μm in diameter. The porous spheres were saturated with electrolyte solution (5×10^{-3} M $CaCl_2$) for several days and were packed into a glass column (Ace Glassware, 7.9 cm diameter, 15.0 cm length) along with glass beads. Pure silica glass beads were selected to minimize sorbate interactions so as to focus on the physical nonequilibrium processes. The glass beads (212–300 μm diameter, mean 250 μm, Sigma Chemical Company) were acid soaked for 1 day and then washed with deionized water from NANOpure ultrapure water system until acid free.

Table 1. Properties of the Solutes

Solute	MW	MV*	D_0, cm^2/h	C_0, mg/L
^3H_2O	22	22	0.0878†	···
PFBA	212	144	0.0284‡	100
2,4-D	221	156	0.0243‡	50
HPCD	1500	1875	0.0064‡	2000

MW: molecular weight; MV: molar volume; D_0: diffusion coefficient in water; C_0: influent concentration of solute.

*MV = M.W./density; with densities (grams per cubic centimeter) of 0.8 for HPCD, 1.47 for PFBA, and 1.42 for 2,4-D.

†From *Wang et al.* [1953].

‡Estimated by use of Hayduk and Laudie approach [*Tucker and Nelken*, 1982].

The columns were packed in incremental steps in the presence of the electrolyte solution to establish uniform bulk density. This porous media consisted of a distinct bimodal pore size distribution, consisting of microporosity within the porous spheres and macroporosity between the spheres. This porous medium was intended to represent an idealized aggregated medium with distinct interaggregate and intra-aggregate domains. Two columns with different numbers of porous spheres were packed (see Table 2).

In addition to the glass columns described above, Plexiglas columns were packed with the following porous media: (1) glass beads only and (2) solid glass spheres (0.5 cm radius) dispersed in glass beads. For the latter column the ratios of the volumes of solid spheres to the column volume were the same as the corresponding columns with porous spheres. Data from these columns were used to examine the boundary effects of the column apparatus and the effect of a bimodal particle size distribution on dispersion.

Stratified system. A stainless steel column (7.6 cm diameter, 30.5 cm length, MODcol Corporation) was packed sequentially with two media of differing hydraulic conductivities. First, a central core of 210-μm fine sand was emplaced; the diameter of the core was 4.1 cm. Second, the volume between the core and the column wall was filled with a 840-μm sand. The mass of 840-μm sand represented 74% of the total mass of solids packed in the column. Properties of the column are reported in Table 2.

A miscible displacement experiment was also performed with a column packed with only the 840-μm sand. This column (2.5 cm diameter, 6.35 cm length) had a pore volume of 11.5 cm^3, a bulk density of 1.55 g cm^{-3}, and a porosity of 0.37. This experiment, performed with PFBA, was used to obtain information on the dispersive properties of the coarse sand.

Macroporous system. Preparative chromatography columns made of precision bore stainless steel (2.1 cm diameter, and 7.0 cm length, Alltech Associates, Inc.), with diffusion disks (2 μm pore diameter) at both ends, were used in the experiments with macroporous media. Stainless steel screen (74 μm in pore size) was used to form a cylindrical macropore (0.4 cm inside diameter, 6.2 cm length). This macropore was placed in the middle of the stainless steel column while packing with the glass beads (104 or 37 μm diameter). The columns were packed incrementally in the presence of electrolyte solution to ensure uniform distribution. For the column in which the 37-μm glass beads were packed, a glass microfiber filter (0.7 μm in pore size) was wrapped around the screen to prevent the glass beads from entering the macropore. Properties of the columns are presented in Table 2.

Miscible Displacement

After packing, the columns were slowly wetted from the bottom with electrolyte solution (5×10^{-3} *M* $CaCl_2$ in the aggregated and macroporous system; 10^{-3} *M* $Ca(ClO_4)_2$ in the stratified system) for saturation and to condition them to the electrolyte solution. The columns were positioned vertically, with a HPLC pump (SSI Model 300) connected to the lower end plate of the column. A three-way switching valve was

Table 2. Properties of the Packed Columns and Selected Parameter Values

Porous Media	Column	No.	L	ρ	T	θ	θ_a	θ_n	ϕ	N	a	l
					Homogeneous Media							
Glass beads only	Plexiglas	WQ10	15.0	1.47	223	0.33	0.33	···	1.0	···	···	···
Solid spheres in glass beads	Plexiglas	WQ11	15.0	1.72	204	0.30	0.30	···	1.0	0.37	···	···
Solid spheres in glass beads	Plexiglas	WQ12	15.0	1.89	177	0.26	0.26	···	1.0	0.71	···	···
					Aggregated Media							
Porous spheres in glass beads	glass	WQ13	15.0	1.60	267	0.37	0.30	0.07	0.81	0.28	15	0.55
Porous spheres in glass beads	glass	WQ14	15.0	1.66	262	0.36	0.23	0.13	0.63	0.53	15	0.55
Porous spheres in glass beads	Plexiglas	WQ18	15.0	1.65	263	0.39	0.25	0.14	0.64	0.57	15	0.55
					Stratified Media							
210-μm and 840-μm sand	stainless steel	WQ15	30.5	1.44	680	0.49	0.36	0.13	0.74	···	12	2.01
					Macroporous Media							
Macropore in 104-μm sand	stainless steel	WQ16	7.0	1.48	9.3	0.38	0.03	0.35	0.08	···	···	···
Macropore in 37-μm sand	stainless steel	WQ17	7.0	1.46	10.0	0.40	0.03	0.37	0.08	···	···	···

L is column length (centimeters); ρ is bulk density (grams per cubic centimeter); T is column pore volume (cubic centimeters); θ is fractional pore water content (a, n denoting advective and nonadvective, respectively); $\phi = \theta_a/\theta$; N is number of spheres per column volume (number per cubic centimeter); a is shape factor; l is characteristic length (centimeters).

placed in line to facilitate switching between solutions with and without the solute of interest. A flow-through, variable-wavelength UV detector (Gilson Model 115, 235 nm) was used to continuously monitor concentrations of PFBA or 2,4-D in the column effluent. The transport of HPCD was analyzed by measuring the fluorescence of HPCD complexed with TNS (2-*p*-toluidinnaphthalene-6-sulfonate) in a flow-through fluorometer (excitation filter, 305–395 nm; emission filter, 430–470 nm) (Gilson Model 121). Output of flow-through experiments was recorded on a strip chart recorder (Fisher Recordall Series 5000 or Kipp & Zonen model BD41). The initial concentrations of solutes used in the experiments are listed in Table 1.

For the experiments with ^3H_2O, column effluent fractions were collected with an automated fraction collector (Pharmacia RediFrac or ISCO Retriever), and the activities for ^3H_2O in the effluent samples were analyzed by radioassay using liquid scintillation counting (Packard Tri-Carb Liquid Scintillation Analyzer, Model 1600TR). Specific activity of tritium in the displacing solution was 2.5 nCi/mL (in the aggregated and the macroporous systems) and 15 nCi/mL (in the stratified system).

Data Analysis

Dual-Porosity Mobile-Immobile Model

For some of the systems analyzed herein we will assume one-dimensional steady state water flow, with advective-dispersive flux confined to the advective domain. The two dimensionless governing equations for the first-order, dual-porosity mobile-immobile (MI) solute transport model are [*van Genuchten and Wierenga*, 1976]

$$\beta R \frac{\partial C_1}{\partial T} + (1 - \beta) R \frac{\partial C_2}{\partial T} = \frac{1}{P} \frac{\partial^2 C_1}{\partial X^2} - \frac{\partial C_1}{\partial X} \tag{1}$$

$$(1 - \beta) R \frac{\partial C_2}{\partial T} = \omega (C_1 - C_2) \tag{2}$$

Definitions of the parameters in (1) and (2) are as follows:

$$T = vt/L = v_a t \phi / L \tag{3a}$$

$$X = x/L \tag{3b}$$

$$\phi = \theta_a/\theta \qquad \theta = \theta_a + \theta_n \tag{3c}$$

$$C_1 = C_a/C_0 \qquad C_2 = C_n/C_0 \tag{3d}$$

$$P = v_a L/D \qquad v_a = \frac{q}{\theta_a} \tag{3e}$$

$$\omega = \alpha L/v_a \theta_a = \alpha L/q \tag{3f}$$

$$R = 1 + (\rho K_p/\theta) \tag{3g}$$

$$\beta = (\theta_a + \rho f K_p)/(\theta + \rho K_p) \tag{3h}$$

where C_a and C_n are the aqueous phase concentrations for the advective and nonadvective domains ($M\ L^{-3}$), C_0 is the input concentration, v is the average pore water velocity ($L\ T^{-1}$) (with $v_a = q/\theta_a$, the velocity in the advective domain), q is Darcy flux ($L\ T^{-1}$), t is time, x is distance, L is column length, D is the local-scale dispersion coefficient for the advective domain ($L^2\ T^{-1}$), ρ is bulk density of the porous media in the column ($M\ L^{-3}$), θ is volumetric water content (with subscripts a and n representing advective and nonadvective domains, respectively), f is the fraction of sorbent associated with the advective domain, K_p is the equilibrium sorption coefficient ($L^3\ M^{-1}$), and α is the first-order mass transfer coefficient (T^{-1}).

Parameter Determination

The preferred method by which to evaluate a model is to compare model predictions to experimental data, with all model parameters obtained independently. To do this, values must be obtained for four parameters: R, P, β, and ω; the input pulse, T, is known from the experiment. For all cases, R was evaluated by mass balance (area above the curve or first moment); R values are listed in Table 3. Values are equal or close to 1 for all cases.

For the aggregated system, values for the Peclet number were based on the results of the miscible displacement experiment for PFBA transport in the column packed with glass beads and solid glass spheres. This data set was analyzed with the traditional advection-dispersion equation, with the value for P being optimized. For WQ14, the Peclet number was fixed at 90 (dispersivity, 0.17 cm). The Peclet number was 106 (dispersivity, 0.14 cm) for WQ11 and 40 (dispersivity, 0.37 cm) for WQ13. For the stratified system the Peclet number was based on the results of PFBA transport in the column packed homogeneously with 840-μm sand. The dispersivity (0.1 cm) calculated from the optimized P was used to estimate P values for the stratified system.

The β term represents the fraction of the solute retention that occurs "instantaneously." Note from (3h) that $\beta = \phi$ when there is no sorption (i.e., $K_p = 0$). For columns packed with the porous spheres, the total volume of water within the porous spheres and also that between the glass beads was gravimetrically measured by oven-drying the two media separately at 110°C. These measurements were then used to calculate the volumetric water contents associated with the interaggregate and intra-aggregate pore water regions (i.e., θ_a and θ_n, respectively). Thus the fraction of the total water content residing in the interaggregate region, ϕ, in each column could be calculated. Gravimetrically determined θ_n values were nearly the same as those calculated by using the average porosity of 0.365 cm^3/cm^3 for porous spheres and the total number of porous spheres in the columns. Values for ϕ are listed in Table 2.

For the stratified media column the 840-μm sand was assumed to compose the advective domain, whereas the 210-μm sand was assumed to compose the nonadvective domain. With the mass of the 840-μm sand representing 74% of the total mass of solids, the foregoing assumption results in a value of 0.74 for ϕ and for β. For the macroporous media, the macropore is assumed to be the "advective" domain while the pores between the glass beads are assumed to be the "nonadvective" domain. Calculated values for ϕ are reported in Table 2.

The Damkohler number, ω, contains the first-order mass transfer coefficient (α) and represents the mass transfer of solute between the advective and nonadvective domains. The coefficient associated with the first-order model can be related to a diffusion coefficient, based on the Fick's law approach, by employing an equation of the following form [see *van Genuchten*, 1985; *Parker and Valocchi*, 1986; *Brusseau et al.*, 1989a]:

$$\alpha = a D_0 \theta_n / \tau l^2 \tag{4}$$

where a is the shape factor, D_0 is the aqueous diffusion coefficient of the solute ($L^2\ T^{-1}$), l is the characteristic length,

Table 3. Conditions of the Experimental Systems and Selected Parameter Values

Media	Column	Experiment	Solute	q	v	v_a	T^*	R
Aggregated	WQ13	13-1	^3H_2O	5.55	15.2	18.8	7.1	1.1
Aggregated	WQ13	13-2	^3H_2O	5.52	15.1	18.7	8.1	1.0
Aggregated	WQ13	13-3	PFBA	5.43	14.8	18.4	6.6	1.1
Aggregated	WQ13	13-5	2,4-D	5.45	14.9	18.5	6.1	1.0
Aggregated	WQ13	13-6	2,4-D	5.45	14.9	18.5	8.4	1.1
Aggregated	WQ13	13-4	HPCD	5.46	14.9	18.5	12.8	1.0
Aggregated	WQ14	14-1	^3H_2O	5.47	15.3	24.1	5.7	1.1
Aggregated	WQ14	14-2	^3H_2O	5.45	15.2	24.0	5.7	1.1
Aggregated	WQ14	14-3	PFBA	4.10	11.4	17.9	6.7	1.1
Aggregated	WQ14	14-4	HPCD	5.63	15.7	24.8	6.1	1.1
Aggregated	WQ14	14-5	^3H_2O	0.63	1.8	2.8	3.1	1.2
Aggregated	WQ18	18-1	PFBA	6.12	15.8	24.9	4.6	1.0
Aggregated	WQ18	18-2†	^3H_2O	6.07	15.7	24.7	4.5	1.0
Aggregated	WQ18	18-3†	PFBA	6.07	15.7	24.7	4.5	1.0
Aggregated	WQ18	18-4†	^3H_2O	6.05	15.6	24.6	13.2	1.0
Aggregated	WQ18	18-5†	PFBA	6.05	15.6	24.6	13.2	1.1
Stratified	WQ15	15-1	^3H_2O	4.10	8.3	11.7	3.6	1.0
Stratified	WQ15	15-2	PFBA	4.10	8.3	11.7	5.8	1.0
Macropore	WQ16	16-1	^3H_2O	1.44	65.3	···	16.5	1.0
Macropore	WQ16	16-2	PFBA	1.31	59.2	···	4.7	1.0
Macropore	WQ16	16-3	2,4-D	1.26	57.0	···	9.3	1.0
Macropore	WQ17	17-1	^3H_2O	1.51	61.9	···	7.8	1.0
Macropore	WQ17	17-2	PFBA	1.49	61.2	···	10.5	1.0
Macropore	WQ17	17-3	PFBA	1.50	61.4	···	12.9	1.0
Macropore	WQ17	17-4	2,4-D	1.51	61.9	···	20.9	1.0
Macropore	WQ17	17-5	HPCD	1.50	61.5	···	28.1	1.2

R is retardation factor.
*Input pulse.
†Flow interruption experiments.

and τ is the tortuosity factor for the nonadvective domain. A value of 15 is used for the shape factor for the spherical, synthetic aggregates [*Parker and Valocchi*, 1986]. For the column packed with cylindrical stratified media, a is calculated to be 12 (for solid cylinder with length of cylinder equal to 15ℓ) [*van Genuchten*, 1985]. For the aggregated media, l is the radius of porous spheres, whereas l is the half-thickness of the low-hydraulic conductivity layer (i.e., the nonadvective domain) for the stratified media. A value of 2 is used for τ [*Roberts et al.*, 1987; *Brusseau et al.*, 1994]. Equation (4) was used to calculate values for α, which were used as input to (3f) to calculate values for ω. Values for pertinent properties of the experimental systems (a, θ_n, v, and l) are shown in Tables 2 and 3. Predicted values for β and ω are given in Table 4.

The predicted values obtained for the nonequilibrium parameters β and ω are compared to optimized values obtained from curve fitting. The optimization was done by using CFITIM3 [*van Genuchten*, 1981], a nonlinear, least squares optimization program that incorporates (1) and (2). Values for R and P were fixed at independently determined values, leaving β and ω as the two parameters that were optimized. In a second series, β was fixed to the measured values, leaving ω and T values to be fitted. The fitted T values were very close to measured values.

Results and Discussion

Homogeneous System

Stainless steel porous diffusion plates (100 μm pore size, Mott Metallurgical Corporation) were used on both end plates to ensure uniform water and solute movement. Preliminary testing of water movement in a column packed with glass beads was done by using red dye. The results showed that water movement was very uniform inside the column. The performance of the column apparatus was further evaluated by performing a series of transport experiments in the column packed with glass beads. Replicate breakthrough curves for PFBA are shown in Figure 1a. Symmetrical breakthrough curves indicate minimal dispersion associated with the column and the glass beads. The optimized dispersivity of 0.056 cm is indicative of a well-packed homogeneous column. In addition, the results in Figure 1a show excellent replication.

Breakthrough curves for transport of ^3H_2O and PFBA through the column packed with glass beads and solid glass spheres are presented in Figure 1b. Again, the breakthrough curves are very symmetrical, with negligible early breakthrough and tailing. Furthermore, there is no difference between the ^3H_2O and PFBA breakthrough curves, which indicates that diffusion-controlled processes are not significantly affecting solute transport [*Brusseau*, 1993]. These results suggest that the column apparatus performed well with respect to uniform flow conditions and the absence of apparatus-induced dispersion.

Aggregated System

The breakthrough curves obtained for the transport of ^3H_2O, PFBA, 2,4-D, and HPCD through the aggregated-media columns are presented in Figures 2–6. These curves exhibit both early breakthrough and tailing (delayed approach to relative concentrations of 1 and 0), indicative of nonideal transport. As previously mentioned, the reproducibility of the miscible-displacement method was evaluated by comparing the results of replicate experiments. Breakthrough curves of ^3H_2O in column WQ13 and WQ14 are shown as an additional example (see Figures 2a and 2b); good reproducibility of replicates is apparent. The frontal and distal portions of break-

Table 4. Calculated and Optimized Nonequilibrium Parameter Values

		β		ω		α	
Experiment*	Solute	Calculated	Optimized†	Calculated	Optimized	Calculated	Optimized
13-1	^3H_2O	0.81	0.66 (0.65–0.67)	0.42	0.83 (0.71–0.95)	0.15	0.31 (0.26–0.35)
		0.81	0.81	0.42	0.40 (0.32–0.48)	0.15	0.15 (0.12–0.18)
13-2	^3H_2O	0.81	0.61 (0.59–0.63)	0.42	1.20 (1.01–1.39)	0.15	0.44 (0.37–0.51)
		0.81	0.81	0.42	0.44 (0.39–0.49)	0.15	0.16 (0.14–0.18)
13-3	PFBA	0.81	0.88 (0.88–0.88)	0.14	0.10 (0.09–0.11)	0.05	0.04 (0.04–0.04)
		0.81	0.81	0.14	0.20 (0.16–0.24)	0.05	0.07 (0.06–0.08)
13-4	HPCD	0.81	0.54 (0.53–0.55)	0.03	0.50 (0.45–0.55)	0.01	0.18 (0.16–0.20)
		0.81	0.81	0.03	0.04 (0.04–0.04)	0.01	0.01 (0.01–0.01)
13-5	2,4-D	0.81	0.80 (0.79–0.81)	0.12	0.16 (0.13–0.19)	0.04	0.06 (0.05–0.07)
		0.81	0.81	0.12	0.14 (0.12–0.16)	0.04	0.05 (0.04–0.06)
13-6	2,4-D	0.81	0.82 (0.81–0.83)	0.12	0.16 (0.13–0.19)	0.04	0.06 (0.05–0.07)
		0.81	0.81	0.12	0.17 (0.13–0.21)	0.04	0.06 (0.05–0.07)
14-1	^3H_2O	0.63	0.57 (0.55–0.59)	0.78	0.65 (0.61–0.69)	0.28	0.24 (0.22–0.26)
		0.63	0.63	0.78	0.51 (0.43–0.59)	0.28	0.18 (0.16–0.20)
14-2	^3H_2O	0.63	0.58 (0.57–0.59)	0.78	0.61 (0.57–0.65)	0.28	0.22 (0.21–0.23)
		0.63	0.63	0.78	0.57 (0.57–0.57)	0.28	0.21 (0.21–0.21)
14-3	PFBA	0.63	0.64 (0.63–0.65)	0.34	0.24 (0.22–0.26)	0.09	0.06 (0.06–0.06)
		0.63	0.63	0.34	0.27 (0.25–0.29)	0.09	0.07 (0.07–0.07)
14-4	HPCD	0.63	0.61 (0.60–0.62)	0.06	0.28 (0.24–0.32)	0.02	0.11 (0.09–0.13)
		0.63	0.63	0.06	0.20 (0.18–0.22)	0.02	0.07 (0.06–0.08)
18-1	PFBA	0.64	0.66 (0.65–0.66)	0.24	0.19 (0.17–0.21)	0.10	0.08 (0.07–0.08)
		0.64	0.64	0.24	0.22 (0.19–0.24)	0.10	0.09 (0.08–0.10)
15-1	^3H_2O	0.74	0.80 (0.79–0.81)	0.12	0.04 (0.02–0.06)	0.016	0.005 (0.003–0.007)
15-2	PFBA	0.74	0.77 (0.76–0.78)	0.04	0.05 (0.02–0.08)	0.005	0.007 (0.003–0.01)

*Numbers 13–18 denote the column number, and 1–6 the individual experiment.
†Values in parentheses represents 95% confidence intervals.

through curves obtained from this work were compared. For all solutes these comparisons show the two curves to be coincident (figures not shown), indicative of a well-controlled experimental system. This also serves as a check on the mass balances, since coincident curves signify total recovery of the mass that entered the column.

The extent of nonideality is directly related to the number of porous spheres in the column. For example, tailing of the

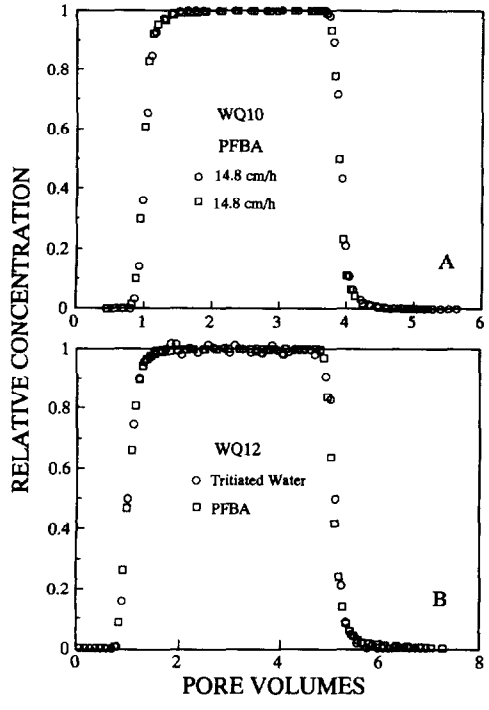

Figure 1. (a) Breakthrough curves for transport of PFBA through the homogeneous glass beads column. (b) Breakthrough curves for transport of tritiated water and PFBA through the column packed with glass beads and solid spheres.

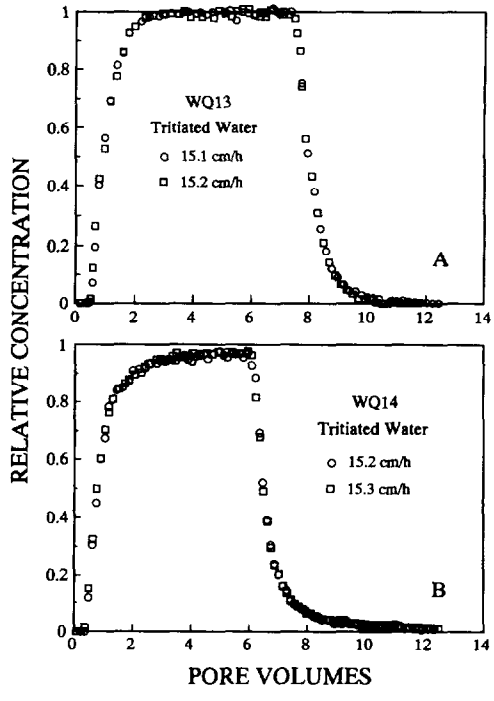

Figure 2. Replication for transport of tritiated water. (a) Breakthrough curves for transport through the aggregated media column (WQ13). (b) Breakthrough curves for transport through the aggregated media column (WQ14).

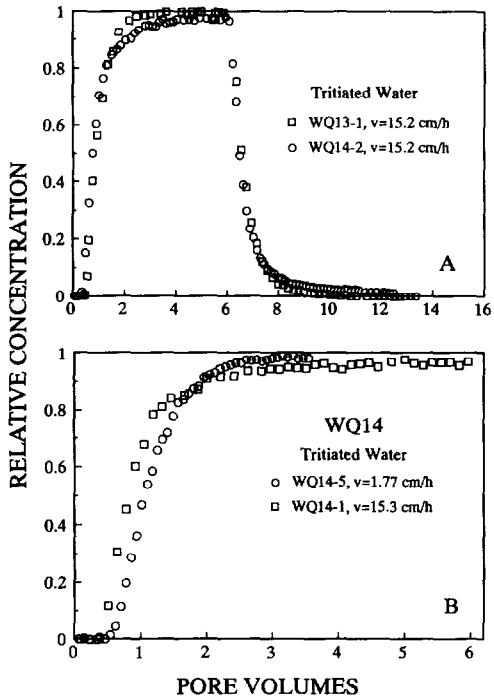

Figure 3. (a) Effect of number of porous spheres on transport of tritiated water in two columns packed with aggregated media. (b) Effect of pore water velocity on transport of tritiated water in aggregated media (column WQ14).

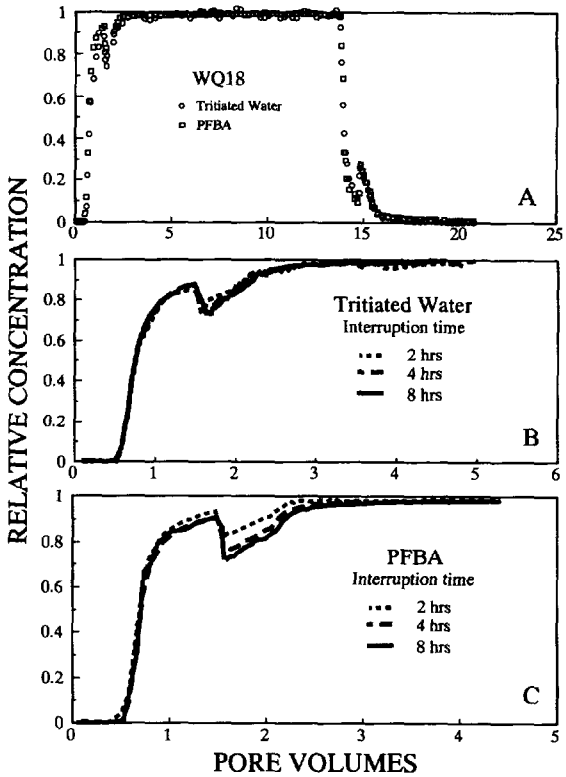

Figure 4. Breakthrough curves for which flow was interrupted during transport in aggregated media (column WQ18): (a) simultaneous transport of tritiated water and PFBA (the flow interruption times are 2 hours for the arrival wave and 8 hours for the elution wave); (b) effect of flow interruption time on concentration change for tritiated water; (c) effect of flow interruption time on concentration change for PFBA.

breakthrough curve for ^3H_2O transport in WQ14 (N = 0.53) is more pronounced than that for WQ13 (N = 0.28) (see Figure 3a). The number of porous spheres in WQ14, which corresponds to the extent of nonadvective domains (microporosity), is nearly twice that in WQ13. Therefore diffusive mass transfer of solute between advective and nonadvective domains has greater impact for WQ14 than for WQ13.

Since diffusive mass transfer is a rate-limited process, residence time is expected to affect nonideality. This is shown in Figure 3b, where breakthrough curves obtained at two pore water velocities are presented. Inspection reveals that the breakthrough curve is more nonideal at the large pore water velocity. Further evidence of the existence of a rate-limited process is provided by the results of flow interruption experiments (Figure 4a), performed following the methods of *Brusseau et al.* [1989b]. A drop in the concentration profile for the arrival wave and a concentration rebound for the elution wave for nonreactive solutes are indicative of transport influenced by a physically related rate-limited process. The preceding results can be attributed to the impact of diffusive transfer of solute between the interaggregate and intra-aggregate pore water regions. Transport in such a system should be influenced by solute size.

Breakthrough curves obtained for all solutes for columns WQ13 and WQ14 are shown in Figures 5 and 6. A comparison reveals that the extent of tailing is in the following order: HPCD > 2,4-D, PFBA > ^3H_2O. For example, the point at which the output concentration equals the input concentration was attained at approximately 11.9, 6.4, 6.8, and 3.8 pore volumes for HPCD, 2,4-D, PFBA, and ^3H_2O, respectively, in the WQ13 system. This trend exhibited by different solutes is consistent with the impact of solute size on the relative degree of nonequilibrium experienced by solutes whose transport is constrained by diffusive mass transfer [*Brusseau*, 1993]. The basis of this effect can be seen by inspecting (4), which shows that α is a function of D_0. For a given fluid the diffusion coefficient is a function of solute properties such as size or molecular weight.

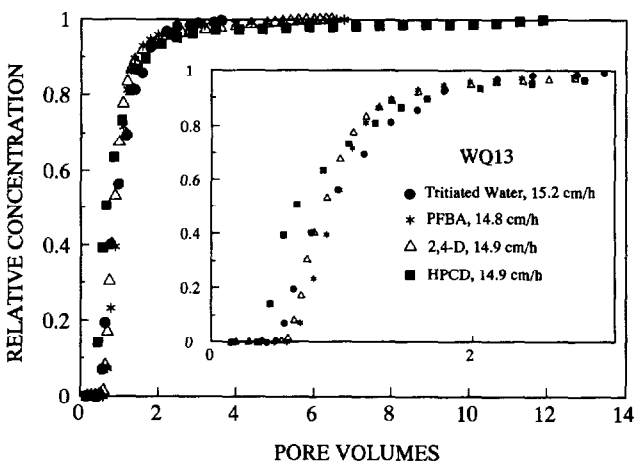

Figure 5. Comparison of breakthrough curves for solutes with different sizes (tritiated water, PFBA, and HPCD) in aggregated media.

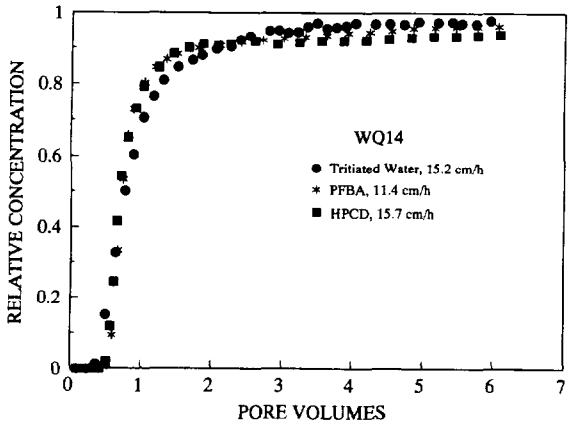

Figure 6. Comparison of breakthrough curves for solutes with different sizes (tritiated water, PFBA, 2,4-D, and HPCD) in aggregated media.

Flow interruption experiments have provided additional evidence regarding the effect of solute size on diffusive transfer of solute between the interaggregate and intra-aggregate pore water regions. The effect of the length of flow interruption on transport of tritiated water and PFBA is shown in Figures 4b and 4c. Flow interruption times of 2, 4, and 8 hours produced similar results for tritiated water; i.e., the magnitudes of the concentration changes were similar for all three interruptions. This indicates that the diffusive mass transfer process reached equilibrium within approximately 2 hours for tritiated water. For PFBA the magnitudes of the concentration change increased with increasing interruption time, indicating nonequilibrium conditions. This difference in behavior is due to the fact that tritiated water has a larger aqueous diffusion coefficient than PFBA.

For most cases the simulations produced with the independently determined values for P, R, β, and ω provided good predictions of the experimental data (see Figures 7 and 8). The optimized simulations produced with the first-order, dual-porosity MI model provided good fits to the data. The one exception is experiment 14-4, which involved transport of HPCD. The optimized curve did not reproduce the extensive tailing exhibited by the data (data not shown). Thus the fitted ω value is suspect. The optimized values for β and ω are reported in Table 4, as are the calculated values. In most cases, especially for PFBA and 2,4-D, the optimized β values are similar to the calculated values. This suggests that the optimized β term does, in fact, represent a real physical entity, i.e., the internal porosity of the aggregates. The predicted ω values are reasonably close to the optimized values; the optimized and calculated ω values differ by a factor of less than 2 in most cases (Table 4). When fixing β to the calculated values, optimized ω values are nearly the same as the calculated ω values, except for HPCD in WQ14 (experiment 14-4).

From (4), it is clear that α is a function only of D_0 (i.e., solute size) for a given system (i.e., constant a, θ_n, τ, and l). Hence the ratio of the α value for a specified solute to that of ^3H_2O should be equal to the ratio of their respective D_0 values. Comparisons between D_0 ratios and the α ratios are presented in Table 5 for the aggregated media. The α ratios are quite comparable to the D_0 ratios for all cases except experiment 14-4 (HPCD). As discussed above, the fitted ω value and, thus, the α value is suspect for this experiment. The generally good

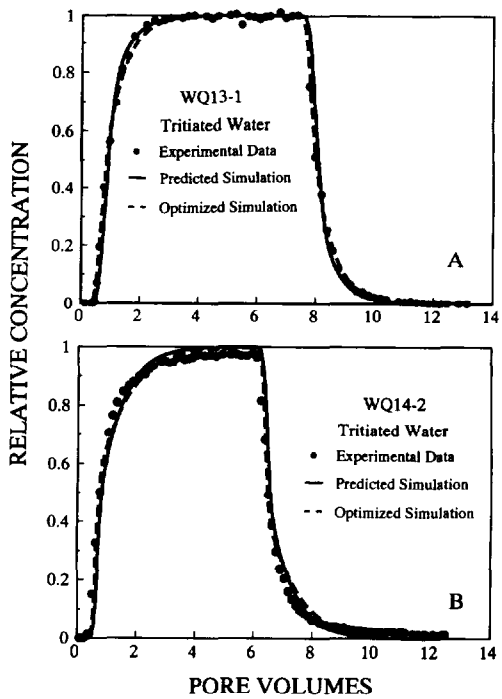

Figure 7. Experimental data and optimized and predicted simulations produced with the first-order, dual-porosity MI model for transport of tritiated water in aggregated media at pore water velocity of 15.2 cm/h: (a) column WQ13; (b) column WQ14.

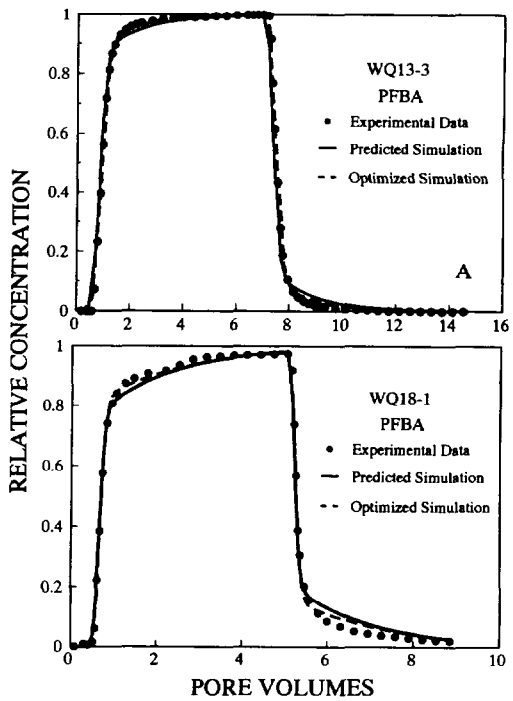

Figure 8. Experimental data and optimized and predicted simulations produced with the first-order, dual-porosity MI model for transport of PFBA in aggregated media: (a) column WQ13, v = 14.8 cm/h; (b) column WQ18, v = 15.8 cm/h.

Table 5. Comparison of α and D_0 Ratios for Aggregated Media

Experiment	Solute	D_0^S/D_0^H	α^S/α^H
13-1,2*	^3H_2O	1.0	...
13-3	PFBA	3.1	2.2
13-4	HPCD	13.7	11.9
13-5	2,4-D	3.6	3.1
13-6	2,4-D	3.6	2.6
14-1,2*	^3H_2O	1.0	...
14-3	PFBA	3.1	2.8
14-4	HPCD	13.7	2.8

The α values obtained from the fixed-β optimization are used for calculation of the ratio. D_0^S is the aqueous diffusion coefficient for the selected solute; D_0^H is the aqueous diffusion coefficient for water; α^S is the mass transfer coefficient for the selected solute. α^H is the mass transfer coefficient for water.

*Average of replicates.

comparisons presented in Table 5 suggest that the impact of solute size on mass transfer and transport can, in this case, be represented quantitatively with the dual-porosity MI model.

Stratified System

The breakthrough curves obtained for the transport of ^3H_2O and PFBA through the stratified-media column are presented in Figure 9. These curves also exhibit both early breakthrough and tailing, indicative of nonideal transport. Comparison of the two curves reveals that the extent of tailing exhibited by PFBA is greater than that exhibited by ^3H_2O. Specifically, the point at which the output concentration equals the input concentration was attained at approximately 3 pore volumes for ^3H_2O and at approximately 6 pore volumes for PFBA. The greater degree

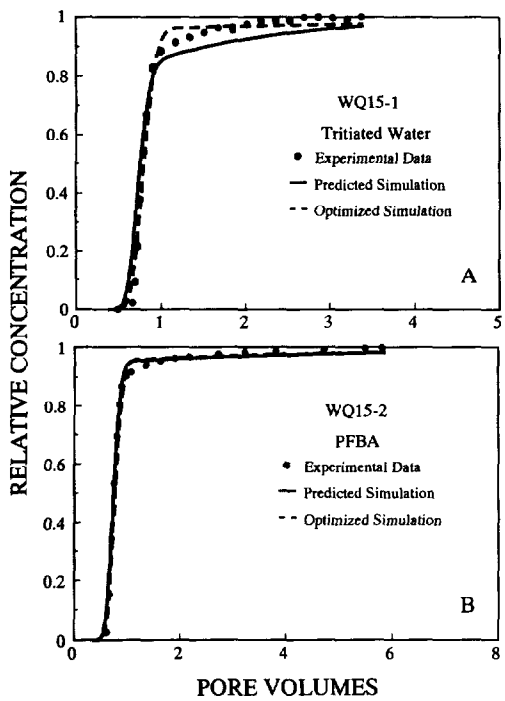

Figure 9. Experimental data and optimized and predicted simulations produced with the first-order, dual-porosity MI model for transport in stratified media (column WQ15): (a) tritiated water; (b) PFBA.

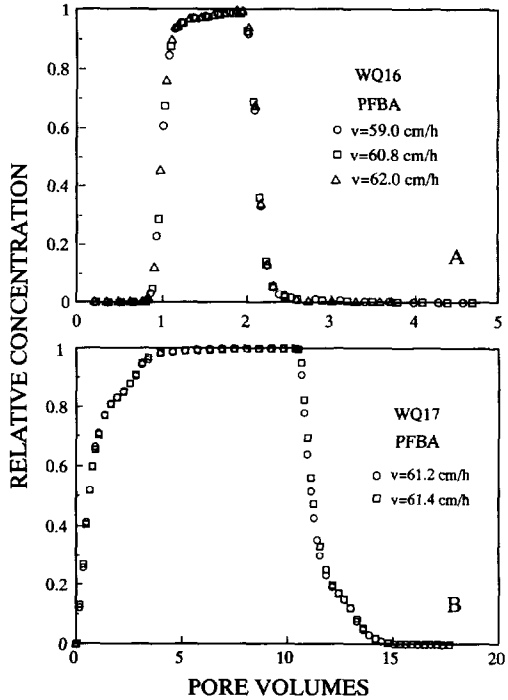

Figure 10. Replication for transport of PFBA. (a) Breakthrough curves through the macroporous media (macropore in 104-μm glass beads). (b) Breakthrough curves for transport through the macroporous media (macropore in 37-μm glass beads).

of nonideality exhibited by PFBA is consistent with the impact of solute size on the diffusive mass transfer process between the advective and nonadvective water domains.

The predicted breakthrough curves simulated with the dual-porosity MI model are compared to the experimental data in Figure 9. The predicted simulations match the experimental data fairly well, especially considering that values for all parameters were obtained independently. The optimized values of β and ω obtained for the data are listed in Table 4. The predicted values are within, or are relatively close to, the 95% confidence intervals of the optimized values. These results suggest that the first-order, dual-porosity MI model can be used to approximate solute transport in this stratified porous medium.

Macroporous System

Breakthrough curves for transport of PFBA in the macroporous media are shown in Figures 10a and 10b; good reproducibility is again apparent. Tailing exhibited by the breakthrough curves indicates nonideal transport in the column with the macropore packed in 104-μm glass beads (WQ16). However, no "early breakthrough" was observed. Conversely, the solutes appeared almost immediately in the effluent for the column with the macropore packed in 37-μm glass beads (WQ17). The abrupt change in shape of the breakthrough curve at $C/C_0 = 0.9$ probably results from transport in the glass bead matrix, whereas the early breakthrough is associated with transport in the macropore.

The breakthrough curves for transport of all solutes in WQ16 and WQ17 are shown in Figures 11 and 12. Inspection reveals that the extent of tailing exhibits the following order: HPCD > 2,4-D, PFBA > ^3H_2O. For column WQ16 the point

at which the output concentration equals the input concentration was attained at approximately 6.7, 5.3, and 3.0 pore volumes for 2,4-D, PFBA and ^3H_2O, respectively. For column WQ17 the point at which the output concentration equals the input concentration was attained at approximately 28.1, 10.2, 8.1, and 4.2 pore volumes for HPCD, 2,4-D, PFBA, and ^3H_2O, respectively. This trend of degree of nonideality exhibited by these different-sized solutes is consistent with the impact of solute size on the diffusive mass transfer process as discussed above.

With the dual-porosity MI model, the porous medium is conceptualized to consist of two domains, an "advective" domain, where advective-dispersive flux occurs, and a "nonadvective" domain wherein advection is negligible. From this assumption, β should be 0.08 for both macroporous columns (see Table 2). However, the fitted β values based on the first-order, dual-porosity MI model are much larger (0.92–0.97 for WQ16; 0.41–0.77 for WQ17), indicative of the failure of the dual-porosity MI model for this system. It is likely that the system is composed of "higher-flow" and "lower-flow" domains, instead of "advective" and "nonadvective" domains.

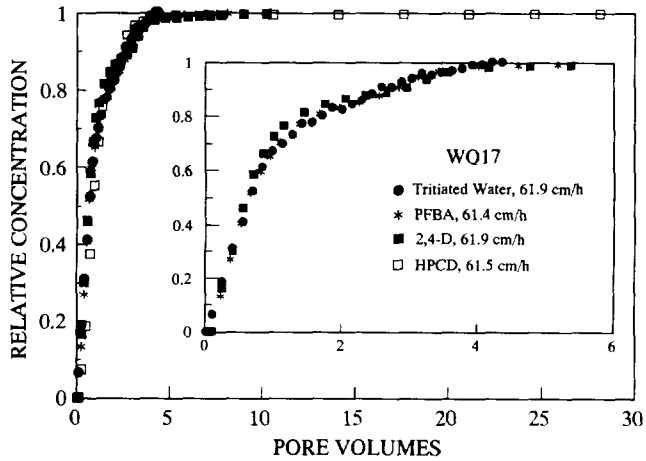

Figure 12. Comparison of breakthrough curves for solutes with different sizes (tritiated water, PFBA, 2,4-D and HPCD) in macroporous media (column WQ17).

Summary and Conclusions

The miscible displacement technique was used to obtain data for the transport of solutes of different sizes in columns packed with aggregated, stratified, and macroporous media. The resultant breakthrough curves exhibited both early breakthrough and tailing, indicative of nonideal transport. Comparison of the curves revealed that the extent of tailing was in the following order: HPCD > PFBA, 2,4-D > ^3H_2O. This behavior is consistent with the impact of solute size on the relative degree of nonequilibrium experienced by solutes where transport is constrained by diffusive mass transfer. The analyses presented above provide evidence that solute size can influence transport in aggregated, stratified, and macroporous media. Hence, performing tracer experiments with solutes of different size would appear to be a good method by which to elucidate the existence of soil structure and to characterize its impact on transport. It must be remembered, however, that solute size is one of several factors (e.g., structure characteristics, pore water velocity) that influences the degree of nonideality observed for solute transport in structured porous media.

Predicted curves simulated with the first-order, dual-porosity mobile-immobile transport model were compared to the experimental breakthrough curves obtained in the aggregated and stratified media. In most cases, the predicted simulations matched the experimental data quite well. Thus it appears that the first-order, dual-porosity MI model can be used to approximate solute transport in aggregated and stratified media, at least for systems similar to those evaluated herein. However, it must be remembered that the dual-porosity approach is a simplification of reality. The binary demarcation of a structured system into advective and nonadvective regions may not be sufficient or appropriate for many systems, such as the macroporous system used in this study.

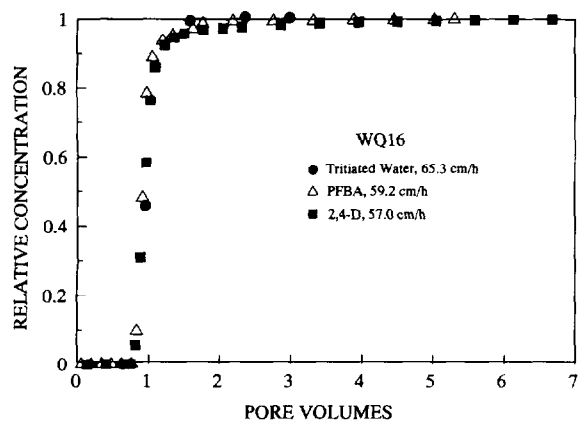

Figure 11. Comparison of breakthrough curves for solutes with different sizes (tritiated water, PFBA, and 2,4-D) in macroporous media (column WQ16).

Acknowledgments. This work was supported in part by projects from the United States Department of Agriculture and the Department of Energy. We thank P. S. C. Rao, University of Florida, who kindly lent us the porous ceramic spheres. A portion of this work was performed under the auspices of the U.S.D.O.E. Faculty Fellow Program (NORCUS), at Battelle/PNL, Washington. The assistance of John Zachara, Jerry Phillips, and Jim Szecsody from Battelle/PNL is greatly appreciated.

References

Biggar, J. W., and D. R. Nielsen, Miscible displacement, II, Behavior of tracers, *Soil Sci. Soc. Am. Proc.*, *26*, 125–128, 1962.

Brusseau, M. L., The influence of solute size, pore water velocity, and intraparticle porosity on solute dispersion and transport in soil, *Water Resour. Res.*, *29*(4), 1071–1080, 1993.

Brusseau, M. L., and P. S. C. Rao, Modeling solute transport in structured soils: A review, *Geoderma*, *46*(1–3), 169–192, 1990.

Brusseau, M. L., R. E. Jessup, and P. S. C. Rao, Modeling the transport of solutes influenced by multiprocess nonequilibrium, *Water Resour. Res.*, *25*(9), 1971–1988, 1989a.

Brusseau, M. L., P. S. C. Rao, R. E. Jessup, and J. M. Davidson, Flow interruption: A method for investigating sorption nonequilibrium, *J. Contam. Hydrol.*, *4*, 223–240, 1989b.

Brusseau, M. L., Z. Gerstl, D. Augistijn, and P. S. C. Rao, Simulating solute transport in an aggregated soil with the dual-porosity model: Measured and optimized parameter values, *J. Hydrol.*, *163*, 187–193, 1994.

Czapar, G. F., R. Horton, and R. S. Fawcett, Herbicides and tracer

movement in soil columns containing an artificial macropore, *J. Environ. Qual.*, *21*, 110–115, 1992.

Herr, M., G. Schafer, and K. Spitz, Experimental studies of mass transport in porous media with local heterogeneities, *J. Contam. Hydrol.*, *4*, 127–137, 1989.

Koch, A., and H. Flühler, Non-reactive solute transport with micropore diffusion in aggregated porous media determined by a flow-interruption method, *J. Contam. Hydrol.*, *14*, 39–54, 1993.

Nkedi-Kizza, P., J. W. Biggar, M. T. van Genuchten, P. J. Wierenga, H. M. Selim, J. M. Davidson, and D. R. Nielsen, Modeling tritium and chloride 36 transport through an aggregated Oxisol, *Water Resour. Res.*, *19*(3), 691–700, 1983.

Parker, J. C., and A. J. Valocchi, Constraints on the validity of equilibrium and first-order kinetics transport models in structured soils, *Water Resour. Res.*, *22*(3), 399–407, 1986.

Passioura, J. B., Hydrodynamic dispersion in aggregated media, 1, Theory, *Soil Sci.*, *111*, 339–344, 1971.

Rao, P. S. C., D. E. Rolston, R. E. Jessup, and J. M. Davidson, Solute transport in aggregated porous media: Theoretical and experimental evaluation, *Soil Sci. Soc. Am. J.*, *44*, 1139–1146, 1980a.

Rao, P. S. C., R. E. Jessup, D. E. Rolston, J. M. Davidson, and D. P. Kilcrease, Experimental and mathematical description of nonadsorbed solute transfer by diffusion in spherical aggregates, *Soil Sci. Soc. Am. J.*, *44*, 684–688, 1980b.

Roberts, P. V., M. N. Goltz, R. S. Summers, J. C. Crittenden, and P. Nkedi-Kizza, The influence of mass transfer on solute transport in column experiments with an aggregated soil, *J. Contam. Hydrol.*, *1*, 375–393, 1987.

Singh, P., and R. S. Kanwar, Preferential solute transport through macropores in large undisturbed saturated soil columns, *J. Environ. Qual.*, *20*, 295–300, 1991.

Southworth, G. R., W. W. Kenneth, and J. L. Keller, Comparison of models that describe the transport of organic compounds in macroporous soil, *Environ. Toxic. Chem.*, *6*, 251–257, 1987.

Sudicky, E. A., R. W. Gillham, and E. O. Frind, Experimental investigation of solute transport in stratified porous media, 1, The nonreactive case, *Water Resour. Res.*, *21*(7), 1035–1041, 1985.

Tucker, W. A., and L. H. Nelken, Diffusion coefficients in air and water, in *Handbook of Chemical Property Estimation Methods: Environmental Behavior of Organic Compounds*, edited by W. J. Lyman, W. F. Reehl, and D. H. Rosenblatt, pp. 17-1 to 17-25, McGraw-Hill, New York, 1982.

van Genuchten, M. T., Nonequilibrium transport parameters from miscible displacement experiments, *Res. Rep. 119*, USDA Salin. Lab., Riverside, Calif., 1981.

van Genuchten, M. T., A general approach for modeling solute transport in structured soils, *Mem. Int. Assoc. Hydrogeol.*, *17*(1), 513–526, 1985.

van Genuchten, M. T., and P. J. Wierenga, Mass transfer studies in sorbing porous media, 1, Analytical solutions, *Soil Sci. Soc. Am. J.*, *40*, 473–480, 1976.

van Genuchten, M. T., and P. J. Wierenga, Mass transfer studies in sorbing porous media, 2, Experimental evaluation with tritium (^3H_2O), *Soil Sci. Soc. Am. J.*, *41*, 272–278, 1977.

Wang, J. H., C. V. Robinson, and I. S. Edelman, Self-diffusion and structure of liquid water, III, Measurement of the self-diffusion of liquid water with H^2, H^3, and O^{18} as tracers, *J. Am. Chem. Soc.*, *75*, 466–470, 1953.

Wang, X., and M. L. Brusseau, Solubilization of some low-polarity organic compounds by hydroxypropyl-β-cyclodextrin, *Environ. Sci. Technol.*, *27*(13), 2821–2825, 1993.

M. L. Brusseau and Q. Hu, Department of Soil and Water Science, 429 Shantz Building, University of Arizona, Tucson, AZ 85721. (e-mail: nonequil@arizvms)

(Received September 9, 1994; revised March 14, 1995; accepted April 6, 1995.)